Original Article

MOLECULAR METABOLISM

# CRISPR/SaCas9 mutagenesis of stromal interaction molecule 1 in proopiomelanocortin neurons increases glutamatergic excitability and protects against diet-induced obesity

**Jian Qiu [1,*], Martha A. Bosch [1], Todd L. Stincic [1,5], Avery C. Hunker [3], Larry S. Zweifel [3,4], Oline K. Rønnekleiv [1,2], Martin J. Kelly [1,2,**]**

## ABSTRACT

**Objective:** Proopiomelanocortin (POMC) neurons are the key anorexigenic hypothalamic neuron for integrating metabolic cues to generate the appropriate output for maintaining energy homeostasis and express the requisite channels as a perfect synaptic integrator in this role. Similar to the metabolic hormones leptin and insulin, glutamate also excites POMC neurons via group I metabotropic glutamate receptors (mGluR1 and 5, mGluR1/5) that activate Transient Receptor Potential Canonical (TRPC 5) Channels to cause depolarization. A key modulator of TRPC 5 channel activity is stromal interaction molecule 1 (STIM1), which is involved in recruitment of TRPC 5 channels from receptor-operated to store-operated calcium entry following depletion of calcium from the endoplasmic reticulum.

**Methods:** We used a single adeno-associated viral (AAV) vector containing a recombinase-dependent *Staphylococcus aureus* Cas9 (SaCas) and a single guide RNA (sgRNA) to mutate *Stim1* in POMC$^{Cre}$ neurons in male mice, verified by qPCR of *Stim1* mRNA expression in single POMC neurons. Whole-cell patch clamp experiments were conducted to validate the effects of *Stim1* mutagenesis. Body weight and food intake were measured in male mice to assess disruptions in energy balance.

**Results:** Reduced *Stim1* expression augmented the efficacy of the mGluR1/5 agonist 3, 5-Dihydroxyphenylglycine (DHPG) to depolarize POMC neurons via a G$\alpha_q$-coupled signaling pathway, which is an essential part of excitatory glutamatergic input in regulating energy homeostasis. The TRPC 5 channel blockers HC070 and Pico145 antagonized the excitatory effects of DHPG. As proof of principle, mutagenesis of *Stim1* in POMC neurons reduced food intake, attenuated weight gain, reduced body fat and fat pad mass in mice fed a high fat diet.

**Conclusions:** Using CRISPR technology we have uncovered a critical role of STIM1 in modulating glutamatergic activation of TRPC 5 channels in POMC neurons, which ultimately is important for maintaining energy balance.



**Keywords** CRISPR/SaCas9; POMC; STIM1; TRPC 5 channel; Glutamate; High fat diet

## 1. INTRODUCTION

Mammalian TRPC channels can be activated by G protein-coupled receptors and receptor tyrosine kinases [1,2] and are one of the major targets for group I metabotropic glutamate receptors (mGluR1/5)-mediated signaling in CNS neurons [3–6]. For example, TRPC 5 channels are highly expressed in substantia nigra dopamine neurons, and mGluR1/5 agonists such as DHPG ((S)-3,5-Dihydroxyphenylglycine) induce an inward current that exhibits a double-rectifying current–voltage plot [3]. Similarly, DHPG depolarizes POMC neurons, and high frequency stimulation of arcuate nucleus kisspeptin (Kiss1$^{ARH}$) neurons releases enough glutamate to "spill over" and activate extrasynaptic metabotropic glutamate (mGluR1/5) receptors [7]. mGluR1/5 are G$\alpha_q$-coupled to phospholipase C (PLC) activation, which leads to hydrolysis of phosphatidylinositol 4,5-bisphosphate ($PIP_2$) to diacylglycerol (DAG) and inositol 1,4,5 triphosphate ($IP_3$) that mediate further downstream actions. One of the targets is the TRPC 5 channel, which is a cation selective channel and can associate with Orai calcium channels to form

[1]Department of Chemical Physiology and Biochemistry, Oregon Health & Science University, Portland, OR 97239, USA [2]Division of Neuroscience, Oregon National Primate Research Center, Beaverton, OR 97006, USA [3]Department of Psychiatry and Behavioral Sciences, University of Washington, Seattle, WA 98195, USA [4]Department of Pharmacology, University of Washington, Seattle, WA 98195, USA

[5] Present address: Department of Biology, Appalachian State University, Boone, NC 28608.

*Corresponding author.Department of Chemical Physiology and Biochemistry, Oregon Health & Science University, Portland, OR 97239, USA E-mail: qiuj@ohsu.edu (J. Qiu).

**Corresponding author.Department of Chemical Physiology and Biochemistry, Oregon Health & Science University, Portland, OR 97239, USA E-mail: kellym@ohsu.edu (M.J. Kelly).

Received September 13, 2022 • Revision received November 9, 2022 • Accepted November 22, 2022 • Available online 25 November 2022

 

calcium release-activated calcium (CRAC) channels [8]. TRPC 5 channels are highly permeable to calcium ($P_{Ca}/P_{Na} = 9:1$) [9], and a unique feature of TRPC 5 (and TRPC 4) channels is that they are potentiated by micromolar concentrations of lanthanum ($La^{3+}$) [10], which we have exploited to characterize TPRC 5 signaling in POMC neurons [11,12]. TRPC channels can function as receptor-operated channels or as store-operated channels depending on their association with the endoplasmic reticulum (ER) protein stromal interaction molecule 1 (STIM1) [8]. STIM1 is localized to the ER membrane of cells and its N-terminal domain contains an EF-hand that protrudes into the lumen of the ER to sense changes in ER $Ca^{2+}$ concentrations [13]. Upon depletion of ER $Ca^{2+}$, STIM1 undergoes a conformational change, oligomerizes and then interacts with plasma membrane TRPC channels [13,14].

Previously, we discovered that the efficacy of insulin to activate TRPC 5 channels and depolarize POMC neurons was significantly reduced in diet-induced obesity male but not female mice [15]. The insulin response in POMC neurons was abrogated in ovariectomized, DIO females but restored with estradiol ($E_2$) replacement—*i.e.,* $E_2$ protected POMC neurons against insulin resistance. Also, $E_2$ downregulated *Stim1* mRNA, which rendered POMC neurons more excitable and more responsive to insulin-mediated TRPC 5 channel activation [15]. In addition, we found that the insulin-induced TRPC 5 current in POMC neurons in ovariectomized females was enhanced in the presence of a store-operated $Ca^{2+}$ channel inhibitor. We have also observed that longer term $E_2$ treatment down-regulates *Stim1* mRNA expression by ~2 fold in the arcuate nucleus of female guinea pigs, indicating that this $E_2$-mediated mechanism for increasing TRPC 5 channel coupling to insulin receptors may be conserved among mammals. Therefore, we hypothesized that under normal physiological conditions, TRPC 5 channels function similarly to other plasma membrane calcium channels in POMC neurons but can also be coupled to plasma membrane receptors (InsR, LRb, mGluR1/5) [7,11,12]. However, in cellular stressed states such as with obesity TRPC 5 channels associate with STIM1 and are coupled to $Ca^{2+}$ store depletion from the endoplasmic reticulum. $E_2$ appears to play a protective role by downregulating *Stim1* mRNA expression. To test this hypothesis, we sought to selectively delete *Stim1* expression in POMC neurons by crossing $Pomc^{Cre}$ mice with $Stim1^{flox/flox}$ mice, thereby producing conditional knockout of *Stim1* in POMC neurons. We had previously used this strategy to delete *Stim1* from $Kiss1^{ARH}$ neurons [16]. However after extensive breeding over some twenty litters, we were unable to generate viable $Pomc^{Cre}::Stim1^{-/-}$ offspring, even though we were able to produce $Kiss1^{Cre}::Stim1^{-/-}$ offspring that survived well into adulthood [16]. Therefore, we took advantage of a newly developed CRISPR technology [17,18] in which we utilized a single adeno-associated viral (AAV) vector containing a recombinase-dependent *Staphylococcus aureus* Cas9 (SaCas) and a single guide RNA (sgRNA) to selectively mutagenize *Stim1* in POMC neurons in male mice and measure changes in both cellular excitability and the whole animal physiological responses to high fat dieting.

## 2. MATERIALS AND METHODS

### 2.1. Animals and treatments

All the animal procedures described in this study were performed in accordance with institutional guidelines based on National Institutes of Health standards and approved by the Institutional Animal Care and Use Committee at Oregon Health and Science University or the University of Washington, Seattle.

### 2.2. Mice

$Pomc^{Cre}$ (RRID:IMSR_JAX:005965, strain of origin: FVB/N) [19], $Pomc^{EGFP}$ (RRID: IMSR_JAX: 009593, strain of origin: C57BL/6 J) [20] and $Stim1^{fl/fl}$ (RRID: IMSR_JAX: 023,350, strain of origin: B6. Cg-Thy1a) [21] transgenic mice were selectively bred at OHSU. $DAT^{IRESCre}$ (RRID: IMSR_JAX: 006660, strain of origin: not specified) [22] transgenic mice were selectively bred at University of Washington. All animals were maintained under controlled temperature and photoperiod (lights on at 0600 h and off at 1800h) and given free access to food and water. We utilized a well-established, diet-induced obesity mouse model in order to do cellular studies on POMC neurons [23,24]. $Pomc^{Cre}$ mice were put on a high fat diet (HFD, 45% kcal from fat, Research Diets, NJ, D12451) starting at 10 weeks of age for 8 weeks in order to induce diet-induced obesity (DIO). A control group of mice received normal grain-based chow (5L0D; Lab Diets). After 7–8 weeks, we prepared coronal slices from both groups of mice and did whole-cell patch recordings from $Pomc^{Cre}$ (POMC) neurons.

### 2.3. Generation and validation of AAV1-FLEX-SaCas9-U6-sg*Stim1*

The sgRNA for targeted mutagenesis of *Stim1* exon 3 was designed as previously described [17]. Oligos (Sigma) for the sgRNA were cloned into pAAV-FLEX-SaCas9-U6-sgRNA (Addgene 124,844). *Stim1* forward: CACCGAAACATAGCACCTTCCATGGT; *Stim1* reverse: AAACACCATGGAAGGTGCTATGTTTC. The control sgRNA oligos contained a three base pair substitution located at the seed region upstream of the PAM. Stim1TTA control forward: CACCGAAACATAGCACCTTCCATTTA; Stim1TTA control reverse: AAACTAAATGGAAGGTGCTATGTTTC. For targeted deep sequencing of the *Stim1* locus: AAV1-FLEX-SaCas9-U6-sg*Stim1* and AAV1-FLEX-EGFP-KASH were co-injected into the ventral tegmental area (VTA) of $DAT^{Cre}$ mice. Four weeks following surgery, tissue punches of the ventral midbrain from 3 mice were pooled and nuclei were isolated by FACS as described previously [17]. For nuclear isolation, brain tissue was homogenized in buffer containing the following (in mM): 320 Sucrose (sterile filtered), 5 $CaCl_2$ (sterile filtered), 3 Mg(Ac)2 (sterile filtered), 10 Tris pH 7.8 (sterile filtered), 0.1 EDTA pH 8 (sterile filtered), 0.1% NP40, 0.1 Protease Inhibitor Cocktail (PIC, Sigma), 1 β-mercaptoethanol. Optiprep density gradient medium (5 ml of 50%, Sigma) containing (in mM): 5 $CaCl_2$ (sterile filtered), 3 Mg(Ac)2 (sterile filtered), 10 Tris pH 7.8 (sterile filtered), 0.1 PIC, 1 β-mercaptoethanol was added to the homogenate and mixed by inversion. The mixture was loaded onto 10 ml of 29% iso-osmolar Optiprep solution and centrifuged at 7500 RPM for 30 min at 4 °C. The pellet was resuspended in sterile 1xPBS and nuclei were sorted using a BD AriaFACS III, followed by whole genome amplification (WGA) using REPLI-g Advanced DNA Single Cell kit (Qiagen) according to manufacturer's instructions. Two rounds of targeted PCR were performed using the following primer sets. Primer set 1 forward: TAGTGCATTGGAACTGTG; primer set 1 reverse: CCATGTCCTTCTAAGGAC; primer set 2 forward: CTGGAGACAAGTGACTTG; primer set 2 reverse: CTATTCATCCTCTCTCTC. A 260 base pair amplicon from primer set 2 was gel extracted and submitted for deep sequencing (Amplicon-EZ, Genewiz).

### 2.4. AAV delivery to $Pomc^{Cre}$ mice

To visualize the quality and location of the injection/infection, the CRISPR/SaCas9 vector was spiked with a high titer virus encoding mCherry or YFP. The resulting mixture allowed a single injection of both viruses at a similar titer. Co-injected viruses were always the same serotype (AAV1) so as not to affect the transduction efficiency [17]. Three to eight weeks prior to each experiment, the $Pomc^{Cre}$ mice

 

(>60 d old) received bilateral ARH injections of a Cre-dependent adeno-associated viral (AAV; serotype 1) vector encoding yellow fluorescent protein, YFP (AAV1- EF1a-YFP), or mCherry mCh (AAV1-EF1a-mCh) either alone or coinjected with an AAV1 designed to encode SaCas9 and a single-guide RNA (sgRNA) (See the SaCas9 section for specifics on the sgRNA design) or GCaMP6s (AAV9-Syn-Flex-GCaMP6s-WPRE-SV40; Addgene, #100845-AAV9). Using aseptic techniques, anesthetized mice (1.5% isoflurane/O2) received a medial skin incision to expose the surface of the skull. The glass pipette (Drummond Scientific #3-000-203-G/X) with a beveled tip (diameter = 45 μm) was filled with mineral oil, loaded with an aliquot of AAV using a Nanoject II (Drummond Scientific). ARH injection coordinates were anteroposterior (AP): −1.20 mm, mediolateral (ML): ±0.30 mm, dorsoventral (DL): −5.80 mm (surface of brain z = 0.0 mm); 500 nl of the AAV ($2.0 \times 10^{12}$ particles/ml) was injected (100 nl/min) into each position, and the pipette left in place for 10 min post-injection, then slowly retracted from the brain. The skin incision was closed using Vetbond (3 M) and each mouse received analgesia (Rimadyl, 4–5 mg/kg, *s. c.*).

### 2.5. Calcium imaging

For calcium imaging, coronal arcuate slices (250 μm) were prepared from intact *Pomc*$^{Cre}$ males which had received bilateral ARH injections of a Cre-dependent adeno-associated viral (AAV; serotype 1) vector encoding GCaMP6s (RRID:Addgene_100,842) two to three weeks prior to the experiments as previously described [16]. The brain slices were placed in a RC-22C slide recording chamber (Harvard/Warner Instruments) and imaged on an inverted Nikon TiE microscope equipped with a Yokogawa CSU-W1 spinning disk confocal head, integrated under NIS Elements v4.20 (Nikon). The preparation, kept at 32 °C via a cage incubator (Okolab), was continuously perfused with oxygenated artificial CSF (aCSF) at a flow rate of 1.25 ml/min. Images were acquired on a Zyla v5.5 sCMOS camera (Andor) at 0.5 Hz frame-rate, through an 10 × (NA 0.45) or 20 × (NA 0.75) objective, combining 488 nm laser excitation with 500- to 550-nm emission collection. A single focal plane (z-axis) was maintained using the Nikon Perfect Focus System. Minor tissue drift in the x-y-axis was corrected using NIS Elements. Imaging displaying major drift were excluded from final analysis. Changes in POMC neuron $Ca^{2+}$ levels were measured in regions of interest (ROIs) comprising the GCaMP6s positive cell bodies. In all recordings, background fluorescence measured in an ROI drawn on nearby tissue was subtracted from every ROI. $[Ca^{2+}]_i$ variations after drug applications were assessed as changes in fluorescence signals over baseline ($\Delta F/F_0$). To normalize the fluorescence value of each cell, we first separated experimental trials into two parts: a baseline period (2 min) corresponding to all the frames recorded before addition of drugs, and a stimulus period, after the onset of the drug (such as bath-applied DHPG) application and lasting several minutes. Next, for each ROI we calculated $\Delta F/F_0$ for each frame (t), where $\Delta F/F_0$ equals $(F_{(t)} - F_0)/F_0$, and $F_0$ was the mean fluorescence value for that ROI for all frames in the baseline period for that trial. Maximal peak reached after drug application was also measured and used in quantitative analysis. Data were averaged across all POMC neurons in a slice (one to two slices per animal), which were used as the statistical unit over a minimum of three animals per condition.

### 2.6. Visualized whole-cell patch recording

Whole-cell current clamp and voltage clamp recordings were made from *Pomc*$^{Cre}$ neurons as previously described [11,12]. Coronal arcuate slices (250 μm) were prepared from intact males, 10 weeks and older as previously described [11,12]. The slices were then transferred to an auxiliary chamber in which they were kept at room temperature (25 °C) in artificial CSF (aCSF) consisting of the following (in mm): 124 NaCl, 5 KCl, 2.6 $NaH_2PO_4$, 2 $MgSO_4$, 2 $CaCl_2$, 26 $NaHCO_3$, 10 HEPES, 10 glucose, pH 7.4, until recording (recovery for 2 h). A single slice was transferred to the recording chamber at a time and was kept viable by continually perfusing with warm (35 °C), oxygenated aCSF at 1.25 ml/min. Whole-cell patch recordings were made from *Pomc*$^{Cre}$ neurons using an Olympus BX51 W1 fixed stage scope out-fitted with epifluorescence and infrared-differential interference contrast (IR-DIC) video microscopy. Patch pipettes (A-M Systems; 1.5 μm outer diameter borosilicate glass) were pulled on a Brown/Flaming puller (Sutter Instrument, model P-97) and filled with the following solution: 128 mM potassium gluconate, 10 mM NaCl, 1 mM $MgCl_2$, 11 mM EGTA, 10 mM HEPES, 3 mM ATP, and 0.25 mM GTP adjusted to pH 7.3 with KOH; 295 mOsm. Pipette resistances ranged from 3.5 to 4 MΩ. In whole-cell configuration, access resistance was less than 30 MΩ; the access resistance was 80% compensated. The input resistance was calculated by measuring the slope of the I–V relationship curve between −70 and −50 mV. Standard whole-cell patch recording procedures and pharmacological testing were performed as previously described [11]. Electrophysiological signals were digitized with a Digidata 1322 A (Axon Instruments) and the data were analyzed using p-Clamp software (Molecular Devices, Foster City, CA). The liquid junction potential was corrected for all data analysis. I–V relationships of the drug-induced *(i.e.,* DHPG) currents were constructed by voltage ramps from −100 to +10 mV from a holding potential of −60 mV.

### 2.7. Electrophysiological solutions/drugs

A standard artificial cerebrospinal fluid was used [11]. All drugs were purchased from Tocris Bioscience unless otherwise specified. TTX was purchased from Alomone Labs (1 mM), DL-amino-5-phosphonovaleric acid (AP5; 50 mM), 6-cyano-7-nitroquinoxaline-2,3-dione (CNQX; 10 mM) and Selective group I mGluRs agonist, (S)-3,5-Dihydroxyphenylglycine (DHPG, 50 mM) were dissolved in $H_2O$. Picrotoxin (100 mM), TRPC4/5 antagonist HC070 and TRPC1/4/5 antagonist Pico145 (from MedChemExpress, 10 mM), and Calcium release-activated $Ca^{2+}$ (CRAC) channel Inhibitor GSK7975A (10 mM) from AOBIOUS Inc. (Gloucester, MA) were prepared in dimethylsulfoxide (DMSO). Aliquots of the stock solutions were stored as appropriate until needed.

### 2.8. Glucose tolerance test (GTT)

Mice were housed individually, and body weights were measured once a week. The evening prior to each glucose tolerance test (GTT), all mice were assessed for body composition (fat and lean mass) using a portable digital balance (Ohaus Scout Pro, Bradford, MA) and an EchoMRI 4-in-1-500 Body Composition Analyzer (Houston, TX). Food intake was determined as grams of diet consumed per day. All mice were given either a regular chow diet or a 45% fat diet at 10 weeks of age. Age-matched control and DIO mice were fasted for 15-h and baseline glucose levels measured with the aid of an Accu-Check Advantage blood glucose meter (Roach) using blood collected from the tail vein. Mice were injected intraperitoneally with glucose (1 mg/g lean mass as determined by MRI) [25] in sterile PBS and blood glucose levels were measured 15, 30, 60, 90, and 120 min after injection.

### 2.9. Cell harvesting of dispersed *Pomc*$^{EGFP}$ and *Pomc*$^{Cre}$ neurons labeled with YFP and quantitative real-time PCR (qPCR)

Cell harvesting and qPCR was conducted as previously described [26]. The ARH was microdissected from basal hypothalamic coronal slices

 

obtained from intact male *Pomc*$^{EGFP}$ mice (n = 3) and *Pomc*$^{Cre}$ mice (n = 4 animals/group). The dispersed cells were visualized, patched, and then harvested (10 cells/tube) as described previously [26]. Briefly, the tissue was incubated in papain (7 mg/ml in oxygenated aCSF) for 50 min at 37C and washed 4 times in low $Ca^{2+}$ aCSF and two times in aCSF. Gentle trituration with Pasteur pipettes were used to disperse the neurons onto a glass bottom dish. Oxygenated aCSF circulated into the plate keeping the cells clear of debris. Only healthy cells with processes and a smooth cell membrane were harvested. The cells were harvested using the XenoWorks Microinjector System (Sutter Instruments, Navato, CA), which provided negative pressure in the pipette and fine control to draw the cell up into the pipette. Cells were harvested as pools of 10 individual cells/tube.

Primers for the genes that encode for stromal-interaction molecule 1 (*Stim1*), *Stim2* and $\beta$*-actin* were designed using Clone Manager software (Sci Ed Software) to cross at least one intron-exon boundary and optimized as previously described using Power Sybr Green method [26,27]. We have published the primers for β-actin [7] and *Stim1* (*Stim1* primers span the sgRNA and PAM) and *Stim2* [16]. Controls included neuronal pools reacted without reverse transcriptase (RT), hypothalamic RNA reacted with RT and without RT, as well as water blanks. Primers for qPCR were further tested for efficiency ($E = 10^{(-1/m)} - 1$) [26,28,29]. The results were as follows: $\beta$*-actin*, m = −3.465, $r^2$ = 0.95, efficiency = 95%; *Stim1;* m = −3.311, $r^2$ = 0.98, efficiency = 100%. *Stim2;* m = −3.439, $r^2$ = 0.99, efficiency = 95%. qPCR was performed on a Quantstudio 7 Flex Real-Time PCR System (Life Technologies) using Power Sybrgreen (Life Technologies) mastermix according to established protocols [26]. The comparative $\Delta\Delta C_T$ method [28,29] was used to determine values from duplicate samples of 4 μl for the target genes, *Stim1* and *Stim2* and 2 μl for the reference gene $\beta$*-actin* in a 20 μl reaction volume containing 1× Power SYBR Green PCR Master Mix (Applied Biosystems) and 0.5 μM forward and reverse primers. The relative linear quantity was determined using the $2^{-\Delta\Delta CT}$ equation [26]. In order to determine the relative expression levels of target genes in POMC-YFP neurons obtained from controls as compared to mutated animals, the mean Δ CT for the target genes from the control samples were used as the calibrator. For the POMC-EGFP neurons obtained from intact male animals a comparison was made between *Stim1* expression and *Stim2* expression and the mean Δ CT from *Stim1* was used as the calibrator. The data were expressed as *n*-fold change in gene expression normalized to the reference gene $\beta$*-actin* and relative to the calibrator and the mean and standard error of the mean were calculated and used for statistical analysis.

### 2.10. Experimental design and statistical analysis

In visualized whole-cell patch recording experiments, only one recording was made per slice, and a maximum of 3 recordings were made from each *Pomc*$^{Cre}$ mouse. For cell harvesting of dispersed POMC-YFP and POMC-EGFP neurons and quantitative real-time PCR (qPCR) measurements, 10 cells per pool and 4–5 pools from each animal were used. For the mouse body composition, food intake and GTT experiments, and assessment of mouse energy intake, all animal numbers are indicated in the figure legends. Statistical comparisons between two groups were performed using an unpaired two-tailed Student's t-test. Comparisons between more than two groups were performed using the repeated measures, multifactorial ANOVA. If a significant interaction was encountered, we then moved to the one-way ANOVA, followed by the multiple range tests as specified in the appropriate figure legends. All data were analyzed using GraphPad Prism version 6. All data are presented as mean ± standard error of the mean (SEM). Differences were considered statistically significant if the probability of error was less than 5%.

## 3. RESULTS

### 3.1. CRISPR editing of *Stim1* significantly decreases *Stim1* expression

STIM1 is involved in the regulation of activity in cerebellar Purkinje neurons [30,31], dopaminergic neurons [32] and arcuate POMC neurons and *Kiss1* neurons [15]. To elucidate the functional role of STIM1 in *Pomc*$^{Cre}$ neurons, we tried to generate mice that lack STIM1 selectively in *Pomc*$^{Cre}$ neurons (STIM1$^{pko}$) by excising exon 2 [21] of the *Stim1* gene using a mouse line (JAX stock #023350) in which Cre is expressed under the control of a promoter specific for the expression of *Pomc* [19]. To delete Stim1 from *Pomc*$^{Cre}$ neurons we crossed *Stim*$^{fl/fl}$ mice with *Pomc*$^{Cre}$ mice, which yielded mice that were heterozygotes for *Stim1* deletion (Het) in *Pomc*$^{Cre}$ neurons, as well as *Stim1* Het and wild-type (WT) mice that lacked Cre. Unfortunately, *Stim1*$^{pko}$ mice did not survive *in utero*.

To circumvent the deleterious developmental impact of *Stim1* loss of function in *Pomc*$^{Cre}$ cells, we selectively mutated *Stim1* using a single viral vector CRISPR/SaCas9 approach [17] that allows for conditional mutagenesis in the adult nervous system. CRISPR/Cas9 is recognized as an efficient means of generating insertion/deletion (indel) mutations to cause a loss of function in targeted genes [33–35] with minimal off-target effects [36]. Importantly, there is no unexpected CRISPR-Cas9 off-target activity revealed by trio sequencing of gene-edited mice [36], and trio deep-sequencing does not reveal unexpected off-target and on-target mutations in Cas9-edited rhesus monkeys [37]. To inactivate *Stim1*, we generated a guide targeting exon 3. Because of the small size of the ARH and the relatively low number of POMC neurons, we confirmed the efficacy of SaCas9 mutagenesis of *Stim1* in midbrain dopamine neurons as previously described [17]. Briefly, the *DAT*$^{Cre}$ mice were co-injected with AAV1-FLEX-SaCas9- U6-sg*Stim1* and AAV1-FLEX-EGFP-KASH, and tissue was harvested four weeks following surgery. EGFP-positive and -negative nuclei were isolated by FACS and whole genome amplification (WGA) was performed followed by targeted deep sequencing of a PCR amplicon containing the targeted region of *Stim1* (Figure 1A–C). SaCas9 generated numerous insertions and deletions (indels) centered at 3 base pairs upstream of the protospacer adjacent motif (PAM) (Figure 1A *and* ***C-E***).

Based on the promising results of *Stim1* editing by the SaCas9/sgRNA vector in the *DAT*$^{Cre}$ mice, a cohort of *Pomc*$^{Cre}$ mice was given bilateral stereotaxic injections in the ARH of either AAV1-FLEX-SaCas9-U6-sg*Stim1* or a control virus containing the *Stim1* guide with three base pairs in the mutated seed region (SaCas9-control) as previously described [17]. An additional Cre-dependent virus with the same serotype (AAV1) that drove the expression of a fluorophore (YFP or mCherry) was co-administered to visualize the injection quality and facilitate cell harvesting (Figure 1F–G). To determine the impact of mutagenesis on *Stim1* expression in ARH *Pomc*$^{Cre}$ neurons, we performed single cell qPCR to assess nonsense mediated mRNA decay which has been described following targeted CRISPR/SaCas9 mutagenesis [38]. Brain slices were prepared, and cells were harvested as previously described [39] and analyzed with qPCR. In cerebellar Purkinje neurons, STIM1 is more abundant than STIM2 [30], while in hippocampal [40] and cortical neurons [41] STIM2 levels exceed those of STIM1. In ARH- *Pomc*$^{Cre}$ neurons, we found that *Stim1* mRNA is 2.9-fold greater than *Stim2* mRNA (Figure 1H) and CRISPR/SaCas9 mutagenesis significantly reduced *Stim1* mRNA levels in these cells (Figure 1I).

 

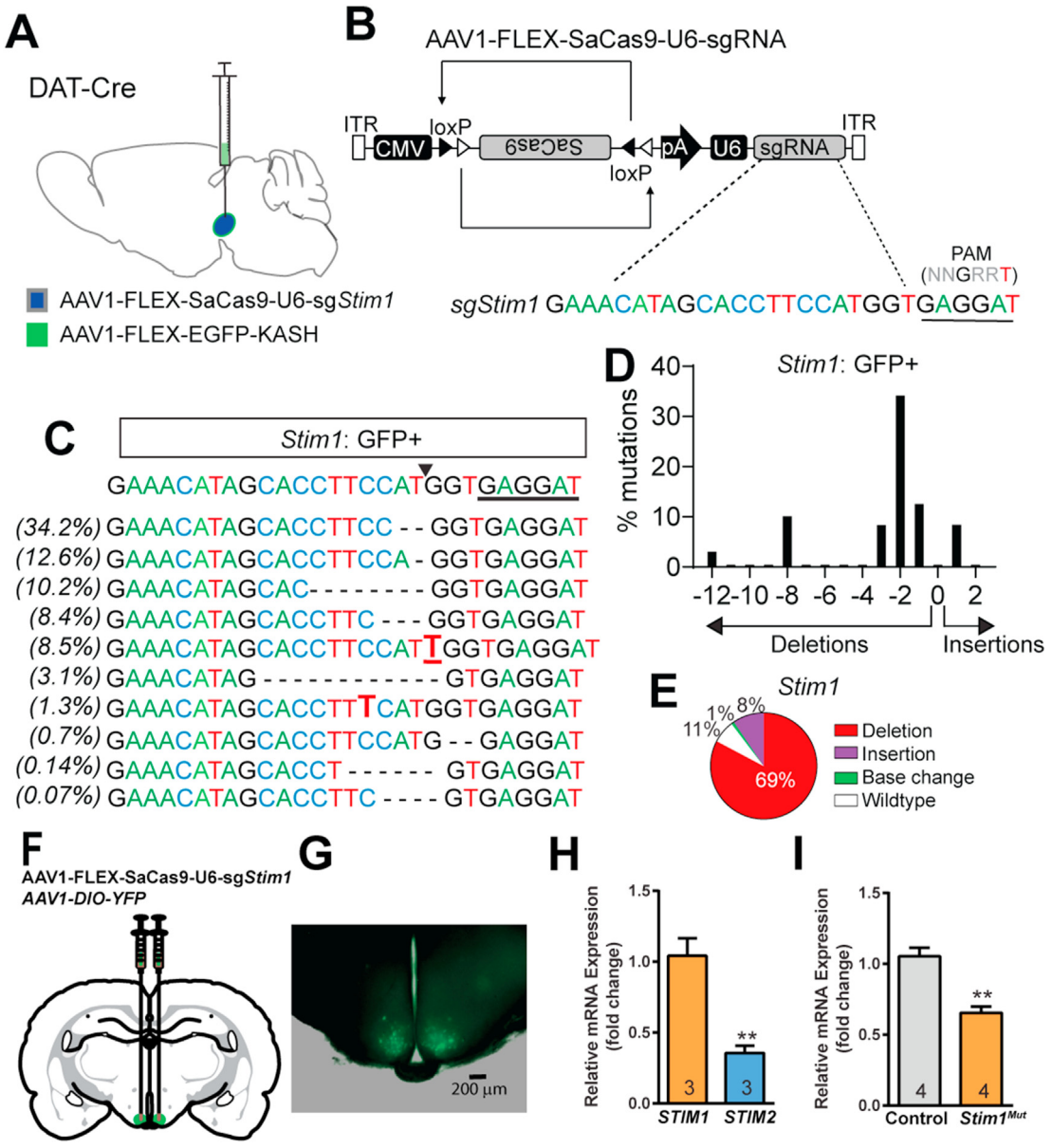


**Figure 1: Analysis of targeted *Stim1* mutagenesis in *DAT*$^{Cre}$ mice and POMC neurons from *Pomc*$^{Cre}$ mice. A**, schematic of a sagittal section showing the viral injections of AAV1-FLEX-SaCas9-U6-sg *Stim1* and control virus into the VTA of adult male *DAT*$^{Cre}$ mice. **B**, design of AAV1-FLEX-SaCas9-U6-sg*Stim1*; the PAM is underlined. **C**, top 10 mutations at the cut site (black arrow) with the percent of total reads for which they occur on the left. Base changes: bolded. Insertions: underlined. Deletions: marked with a "-" (dash). **D**, frequency distribution of insertions and deletions in *Stim1* from GFP$^{+}$ nuclei. **E**, percent of wild-type, deletions, insertions, and base changes as percent of total reads for *Stim1* in GFP$^{+}$. **F**, schematic of a coronal section showing the bilateral viral injections in the ARH with AAV1-DIO-YFP. **G**, photomicrograph showing coronal section confirming targeted bilateral injections of AAV1-FLEX-SaCas9-U6-sg*Stim1* and control virus into the arcuate of adult male *Pomc*$^{Cre}$ mice. Scale, 200 µM. **H**, quantitative PCR assay measuring *Stim1* and *Stim2* in POMC neuronal pools (n = 3 animals, 10 cells per pool, 5 pools/animal) from *Pomc-EGFP* male control mice. Bar graphs represent mean ± SEM (Unpaired *t*-test for the left, $t_{(4)} = 5.092$, $^{**}p = 0.0070$). n = animal number. **I**, quantitative PCR assay measuring *Stim1* in POMC neuronal pools (n = 4 animals, 10 cells per pool, 4 pools/animal) using *STIM1* (135 bp) primers that span the sgRNA and PAM from *Pomc*$^{Cre}$ control and *Stim1*$^{Mut}$ male mice. Bar graphs represent mean ± SEM (Unpaired *t*-test, $t_{(6)} = 5.275$, $^{**}p = 0.0019$).

### 3.2. *Stim1* mutagenesis decreases the excitability of *Pomc*$^{Cre}$ neurons

Recently, we investigated the details of the spike properties in *Kiss1*$^{ARH}$ neurons with deletion of *Stim1* and found that there were no differences between *Kiss1*$^{ARH}$ neurons from control *Kiss1*$^{Cre}$ and *Stim1*$^{kko}$ mice in the firing frequency—current relationship [16]. Nevertheless, in cerebellar Purkinje neurons from *Stim1*$^{pko}$ mice, the firing frequency versus injected current relationship shows a reduced excitability [31]. Based on these observations, we asked whether mutagenesis of *Stim1* with the CRISPR/SaCas9 strategy would alter the activity of these cells. To investigate whether STIM1 modulates the activity of *Pomc*$^{Cre}$ neurons, we bilaterally injected either AAV1-FLEX-SaCas9-U6-sg*Stim1* or a control virus with AAV1-Ef1a-DIO-ChR2:mCherry into the ARH of *Pomc*$^{Cre}$ mice. Initially, whole-cell patch recording in POMC neurons from *Pomc*$^{Cre}$ or *Stim1* mutagenesis (*Stim1*$^{Mut}$) male mice revealed that there was no difference in the resting membrane potential

 

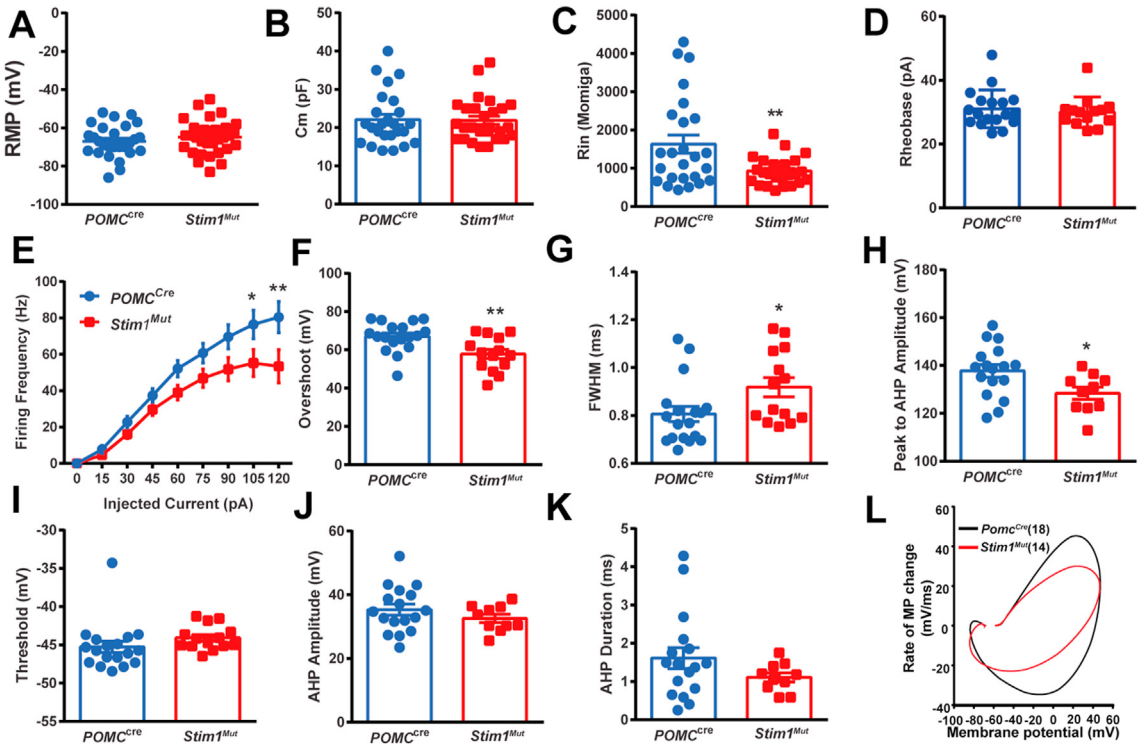


**Figure 2: Electrophysiological properties of POMC neurons from *Pomc*$^{Cre}$ and *Stim1*$^{Mut}$ male mice. A**, Resting membrane potential (RMP)**. B,** Cell capacitance (Cm). **C,** Input resistance (Rin). Unpaired *t*-test, $t_{(49)} = 2.903$, $^{**}p = 0.0055$, *Pomc*$^{Cre}$, n = 25; *Stim1*$^{Mut}$, n = 26**. D,** Rheobase. **E**, firing frequency. There were significant differences in the evoked firing rate between *Pomc*$^{Cre}$ and *Stim1*$^{Mut}$ groups (two-way ANOVA: main effect of treatment, $F_{(1,24)} = 4.464$, $p = 0.0452$, main effect of current, $F_{(8,192)} = 108.7$, $p < 0.0001$, and interaction, $F_{(8,192)} = 3.223$, $p = 0.0018$; *Pomc*$^{Cre}$, n = 13, *Stim1*$^{Mut}$, n = 13; *post hoc* Bonferroni test, $^{*}p < 0.05$ and $^{**}p < 0.01$). **F**, overshot. Unpaired *t*-test, $t_{(30)} = 3.127$, $^{**}p = 0.0039$, *Pomc*$^{Cre}$, n = 18; *Stim1*$^{Mut}$, n = 14**. G,** full width at half maximum (FWHM). Unpaired *t*-test, $t_{(30)} = 2.232$, $^{*}p = 0.0322$, *Pomc*$^{Cre}$, n = 18; *Stim1*$^{Mut}$, n = 14**. H,** Peak to afterhyperpolarization (AHP) amplitude. Unpaired *t*-test, $t_{(25)} = 2.356$, $^{*}p = 0.0266$, *Pomc*$^{Cre}$, n = 17; *Stim1*$^{Mut}$, n = 10**. I**, threshold. **J**, AHP amplitude. **K**, AHP duration. **L**, Phase plots of elicited action potentials.

(Figure 2A) (RMP: *Pomc*$^{Cre}$: 67 ± 1.6 mV, n = 27 vs *Stim1*$^{Mut}$: 64 ± 1.5 mV, n = 32, Unpaired *t*-test, $t_{(57)} = 0.9495$, $p = 0.3464$) or membrane capacitance (Figure 2B) (Cm: *Pomc*$^{Cre}$: 22.1 ± 1.4 pF, n = 25 vs *Stim1*$^{Mut}$: 21.8 ± 1.1 pF, n = 27, Unpaired *t*-test, $t_{(50)} = 0.1322$, $p = 0.8953$). However, there was a significant difference in the membrane input resistance (Figure 2C) (Rin: *Pomc*$^{Cre}$: 1.6 ± 0.2 GΩ, n = 25, vs *Stim1*$^{Mut}$: 0.9 ± 0.0 GΩ, n = 26, Unpaired *t*-test, $t_{(49)} = 2.903$, $p = 0.0055$).), which has also been reported with *Stim1* knockout in both cerebellar Purkinje neurons [31] and arcuate *Kiss1* neurons [16]. To investigate spiking properties, we injected step currents into POMC neurons in current-clamp recordings, and we also measured the rheobase in the presence of synaptic blockers (CNQX, AP5, and picrotoxin) and the frequency–current relationship. The rheobase in POMC control neurons was not different from *Stim1*$^{Mut}$ cells, but the firing frequency versus injected current curve showed a reduced excitability in POMC neurons from *Stim1*$^{Mut}$ mice (Figure 2D–E). Through analysis of the characteristics of single evoked action potentials, we observed that mutagenesis of *Stim1* reduced overshoot and peak to AHP amplitude, but increased full width at half maximum (FWHM) (Figure 2F–H) without affecting threshold, AHP amplitude and AHP duration (Figure 2I–K). However, there was a pronounced decrease in the maximum rise and decay velocity for the generation of an action potential (Figure 2L), which may be driven, in part, by calcium-activated potassium conductances similar to what has been observed in cerebellar Purkinje neurons [31].

### 3.3. The store-operated $Ca^{2+}$ channel inhibitor GSK7975A augments the DHPG-induced current in POMC neurons

Although there appeared to be a decrease in endogenous (autonomous) cell excitability, we hypothesized that POMC neurons may be more coupled to exogenous synaptic input with *Stim1* mutagenesis. Therefore, we explored glutamatergic input and specifically the effects of mGluR1/5 agonist activity. Group I mGluRs (mGluR 1/5) couple to $G\alpha_q$ protein and excite *Pomc*$^{Cre}$ neurons via activation of TRPC5 [7]. Calcium ($Ca^{2+}$) is of critical importance to neurons as it participates in the transmission of the depolarizing signal and contributes to synaptic activity [42]. We first measured the effects of the mGluR1/5 agonist DHPG on GCaMP6s-expressing *Pomc*$^{Cre}$ neurons at different concentrations in arcuate slices from *Pomc*$^{Cre}$ mice. Different concentrations of DHPG (0.5, 5, and 50 μM) were constantly perfused over naïve slices while fluorescence was monitored. DHPG dose-dependently induced an increase in $[Ca^{2+}]_i$ with maximal dose at 50 μM (Figure 3A,B). At 50 μM DHPG, nearly every POMC neuron displayed a rapid and significant increase in fluorescence. The responsivity of POMC neurons to DHPG did not seem to differ based on location, neither medial to lateral within a slice nor rostral caudal between slices. Therefore, we used the mGluR 1/5 agonist DHPG at 50 μM to explore its action in POMC neurons, and found that DHPG induced an inward current in synaptically-isolated POMC neurons in the presence of TTX to block voltage-gated $Na^+$ channels (Figure 3C). We antagonized the effects of DHPG with the selective TRPC4,5 channel blocker

 

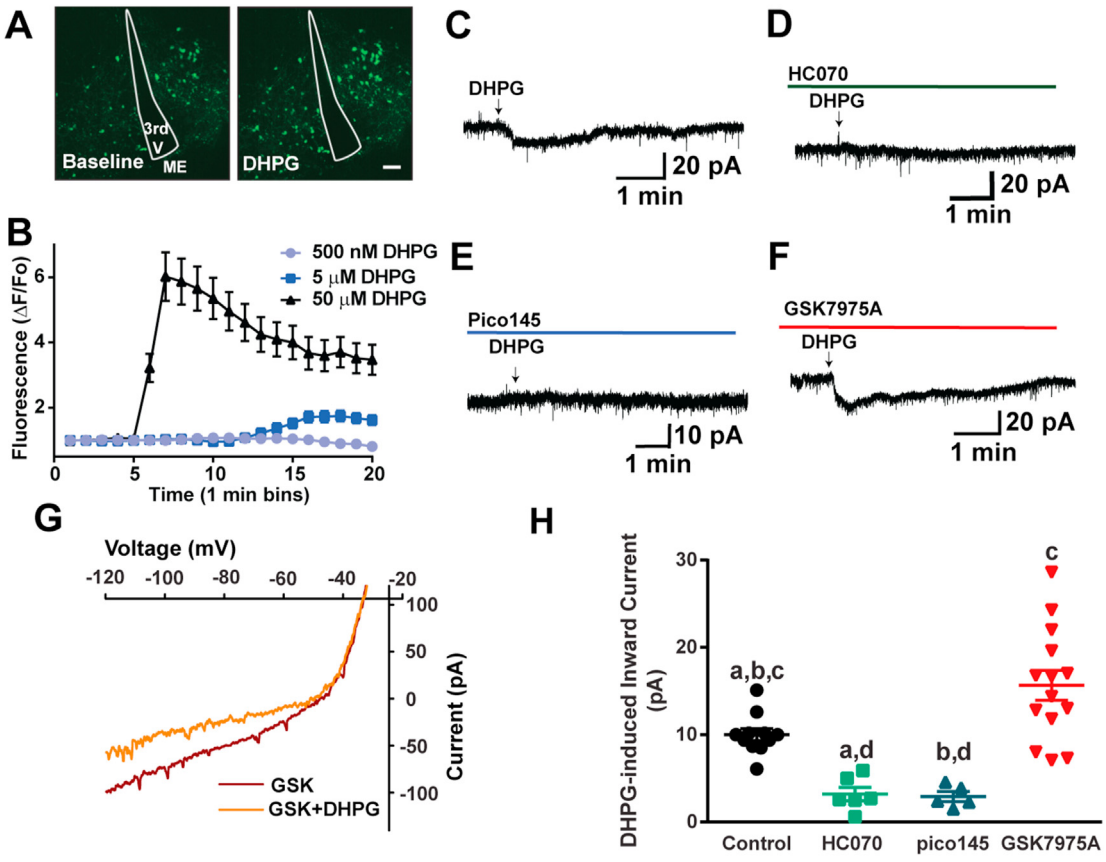


**Figure 3: DHPG-induced current in *Pomc*$^{Cre}$ neurons antagonized by the TRPC5 channel blockers. A-B.** *Ex vivo* calcium imaging of POMC neurons in brain slices. **A,** left panel, spinning disk image of baseline GCaMP6 fluorescence in POMC neurons; right panel, bath perfusion of the mGluR1/5 agonist DHPG (5 μM) significantly increased intracellular $Ca^{2+}$. This concentration is 1/10 of what is typically used *in vitro*, but the effects are still easily measured. Scale bar is 100 μm. **B**, the time course of the responses to increasing concentrations of DHPG represents averaged normalized fluorescence for all cells in a slice (n = 3 slices per concentration). **C-D**, representative traces of DHPG-induced inward current perfused with TTX (1 μM) in the absence (C) or presence (D) of TRPC4/5 channel blocker HC070 (100 nM). **E-F**, representative traces of DHPG-induced inward current perfused with TTX (1 μM) in the presence of TRPC1/4/5 channel blocker Pico 145 (1 μM) (E) or the store-operated $Ca^{2+}$ channel inhibitor GSK7975A (10 μM) (F). 0.1% v/v DMSO vehicle control had no effect (data not shown). DHPG-induced inward currents were recorded in arcuate YFP labeled neurons ($V_{hold}$ = −60 mV) from *Pomc*$^{Cre}$ mice. **G**, the I—V relationship before and during the peak response from the same cell in F indicated that the reversal potential of the nonselective cation current was ~ −30 mV. **H**, summary of the effects of GSK7975A, HC070 and Pico145 on DHPG-induced current (one-way ANOVA, effect of treatment, $F_{(3, 32)} = 16.97$, $p < 0.0001$; *Bonferroni's* multiple comparisons test a,b,c, $p < 0.05$; d, ns.). Scatter plots represent mean ± SEM. n = 11 control, n = 6 HC070, n = 5 pico145 and n = 14 GSK7975A treated neurons.

HC070 [43]. HC070 suppressed the DHPG-induced inward current by 70% in POMC neurons similar to the extent seen with another more selective TRPC 5 channel blocker Pico145 (Figure 3D,E and H) suggesting that DHPG mainly activates TRPC 5 channels. Based on our previous findings that deletion of *Stim1* in hypothalamic arcuate nucleus Kiss1 neurons can augment the TRPC 5 channel conductance [16], we asked whether STIM1 can modulate mGluR1/5 -mediated response. Indeed, in the presence of TTX and the store-operated $Ca^{2+}$ channel inhibitor GSK7975A, the DHPG-induced current was potentiated (Figure 3F,H). The I—V relationship for the response showed a reversal at −30 mV, which is similar to the DHPG-induced current without treatment of GSK7975A (Figure 3G), indicating that the same cationic current is driving the increased conductance.

### 3.4. *Stim1* mutagenesis augments the DHPG-induced current in POMC neurons from mice on a HFD

Our previous findings show that deletion of *Stim1* in hypothalamic arcuate nucleus *Kiss1* neurons protects against diet-induced obesity [16]. In *Kiss1*$^{ARH}$ neurons, conditionally deleted *Stim1* augments tachykinin 3 receptor agonist senktide-induced *Kiss1*$^{ARH}$ neuronal excitability through G$\alpha_q$-coupling to TRPC 5 channel activation [16]. Glutamatergic excitation of POMC neurons plays a critical role in regulating energy homeostasis, and the G$\alpha_q$-coupled mGluR1/5 are a critical part of the signaling pathway [7]. *Stim1* mRNA is highly expressed in POMC neurons and in the presence of a store operated $Ca^{2+}$ channel inhibitor GSK7975A, the insulin-induced TRPC 5 current in POMC neurons in OVX females is enhanced [15]. Therefore, we postulated that *Stim1* mutagenesis should increase the excitability of POMC neurons by glutamatergic inputs in mice on a HFD. To test the hypotheses, we measured the DHPG-induced current and found that in the presence of TTX, DHPG induced an inward current in POMC neurons from Stim1$^{Mut}$ mice on a control diet (Figure 4A,C) and from *Pomc*$^{Cre}$ and *Stim1*$^{Mut}$ mice on a HFD (Figure 4D,F, I). All DHPG-induced inward currents were suppressed by HC070 (Figure 4B,C, E, G, I). In addition, the I—V relationship for the response in POMC neurons from *Stim1*$^{Mut}$ mice on a HFD showed a reversal at −30 mV, which is similar to the DHPG-induced current in a POMC neurons from mice on a control diet (Figure 4H). As we had hypothesized S*tim1* mutagenesis not only augmented the DHPG-induced current in POMC neurons from mice on a HFD (Figure 4I), but it also generated a larger current in POMC neurons

 

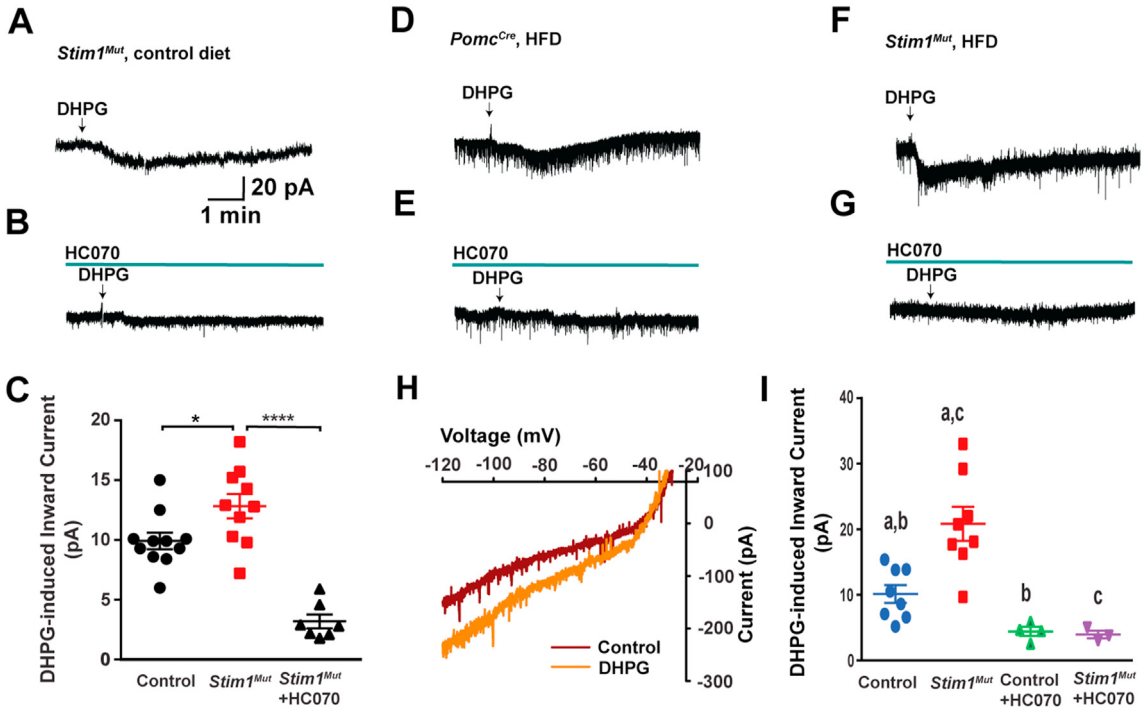


**Figure 4:** *Stim1* mutagenesis augments the DHPG-induced current in POMC neurons from mice on a HFD, which is antagonized by the TRPC4/5 channel blocker HC070. **A-B**, representative traces of DHPG-induced inward current perfused with TTX (1 μM) in the absence (A) or presence (B) of HC070 (100 nM) in POMC neurons on a control diet. $V_{hold} = -60$ mV. **C**, summary of the effects of HC070 and/or *Stim1* mutagenesis on DHPG-induced current in POMC neurons from mice on a control diet (Unpaired *t*-test for control versus $Stim1^{Mut}$, $t_{(19)} = 2.406$, $^{*}p = 0.0264$; Unpaired *t*-test for $Stim1^{Mut}$ versus $Stim1^{Mut}$ + HC070, $t_{(15)} = 7.339$, $^{****}p < 0.0001$). **D-E**, representative traces of DHPG-induced inward current perfused with TTX (1 μM) in the absence (D) or presence (E) of HC070 (100 nM) in POMC neurons from $Pomc^{Cre}$ mice on a HFD. **F-G**, representative traces of DHPG-induced inward current perfused with TTX (1 μM) in the absence (F) or presence (G) of HC070 (100 nM) in POMC neurons from $Stim1^{Mut}$ mice on a HFD. **H**, under voltage clamp conditions, the I/V curve revealed that DHPG generated an inward current that reversed at approximately −30 mV (POMC neuron from F). The kinetics of the I/V curve is similar to controls and treated with GSK7975A (Figure 3G) *I*. Summary of the effects of HC070 on the DHPG-induced inward current in POMC neurons from $Pomc^{Cre}$ and $Stim1^{Mut}$ mice on a HFD (two-way ANOVA, interaction, $F_{(1, 19)} = 5.809$, $p = 0.0262$; effect of strains, $F_{(1, 19)} = 4.834$, $p = 0.0405$; effect of drugs $F_{(1, 19)} = 23.70$, $p = 0.0001$; Bonferroni's multiple comparisons test, a,b,c, $p < 0.05$, n = 8 control, n = 8 $Stim1^{Mut}$, n = 4 Control + HC070 and n = 3 $Stim1^{Mut}$ + HC070 treated neurons.

in mice on a control diet (control: 10.0 ± 0.7 pA, n = 11, versus $Stim1^{Mut}$: 12.9 ± 1.0 pA, n = 10) (Figure 4C).

### 3.5. *Stim1* mutagenesis in $Pomc^{Cre}$ neurons protects male mice against diet-induced obesity

To assess the impact of *Stim1* mutagenesis in ARH-$POMC^{Cre}$ neurons on diet-induced obesity, two cohorts of male mice, $Stim1^{Mut}$ (n = 8) and the littermate control $Pomc^{Cre}$ (n = 8) mice, were put on a HFD for six weeks after one week of the virus injection at around two and half months of age (see Materials and Methods). Over this time period, there was significantly less gain in body weight by week 5 in the $Stim1^{Mut}$ versus the $Pomc^{Cre}$ mice (30.4 ± 0.8 g, n = 8 vs. 32.9 ± 0.5 g, n = 8; Figure 5A). Moreover, the average fat mass of $Stim1^{Mut}$ mice was significantly lighter than that of $Pomc^{Cre}$ controls by week 4 ($Stim1^{Mut}$ vs $Pomc^{Cre}$ mice fat mass: 5.1 ± 0.6 g, n = 8 vs 7.1 ± 0.8 g, n = 8; Figure 5B). But the lean mass of $Stim1^{Mut}$ mice was significantly more versus the $Pomc^{Cre}$ mice ($Stim1^{Mut}$ vs the $Pomc^{Cre}$ mice lean mass: 23.2 ± 0.7 g, n = 8 vs. 22.9 ± 1.7 g, n = 8; Figure 5C). After 5 weeks on high fat diet, average 24- hour food intake was measured in the $Stim1^{Mut}$ group, and the food intake was reduced (Figure 5D). Then both $Stim1^{Mut}$ and $Pomc^{Cre}$ controls were assessed for glucose tolerance using an intraperitoneal GTT (see Materials and Methods). Both $Stim1^{Mut}$ and $Pomc^{Cre}$ males started at relatively the same blood glucose levels after an overnight fast (Figure 5E, time 0); and after intraperitoneal glucose injection $Stim1^{Mut}$ male mice did not have significantly different glucose levels compared with $Pomc^{Cre}$ males, indicating that $Stim1^{Mut}$ males had the same glucose tolerance compared with $Pomc^{Cre}$ controls. Finally, when both groups were euthanized after 7−8 weeks on HFD and peripheral tissues harvested, the perigonadal fat pad masses were significantly lighter in the $Stim1^{Mut}$ versus the $Pomc^{Cre}$ males ($Stim1^{Mut}$ vs the $Pomc^{Cre}$ Pad: 1368 ± 104 mg, n = 8, vs 1935 ± 208 mg, n = 8, Figure 5F). Overall, these results suggest that mutagenesis of *Stim1* in POMC neurons affords some protection against diet-induced obesity.

## 4. DISCUSSION

For the first time, we were able to assess the function of *Stim1* in ARH-POMC neurons in the adult nervous system. Quantitative scRT-PCR revealed that we effectively reduced *Stim1* mRNA expression by fifty percent, consistent with nonsense-mediated decay following CRISPR/SaCas9 mutagenesis. Reduced *Stim1* mRNA in POMC neurons was associated with reduced food intake, attenuated weight gain and reduced body fat and fat pad mass in male mice fed a high fat diet. At the cellular level, *Stim1* mutagenesis augmented the depolarizing effects of the mGluR1/5 agonist DHPG, and the TRPC 5 channel blockers HC070 and Pico145 antagonized these excitatory effects of the Gαq-coupled receptor. Therefore, utilizing CRISPR technology, we have uncovered a critical role for STIM1 in modulating TRPC 5 channel activity in POMC neurons that ultimately affects the control of energy

 

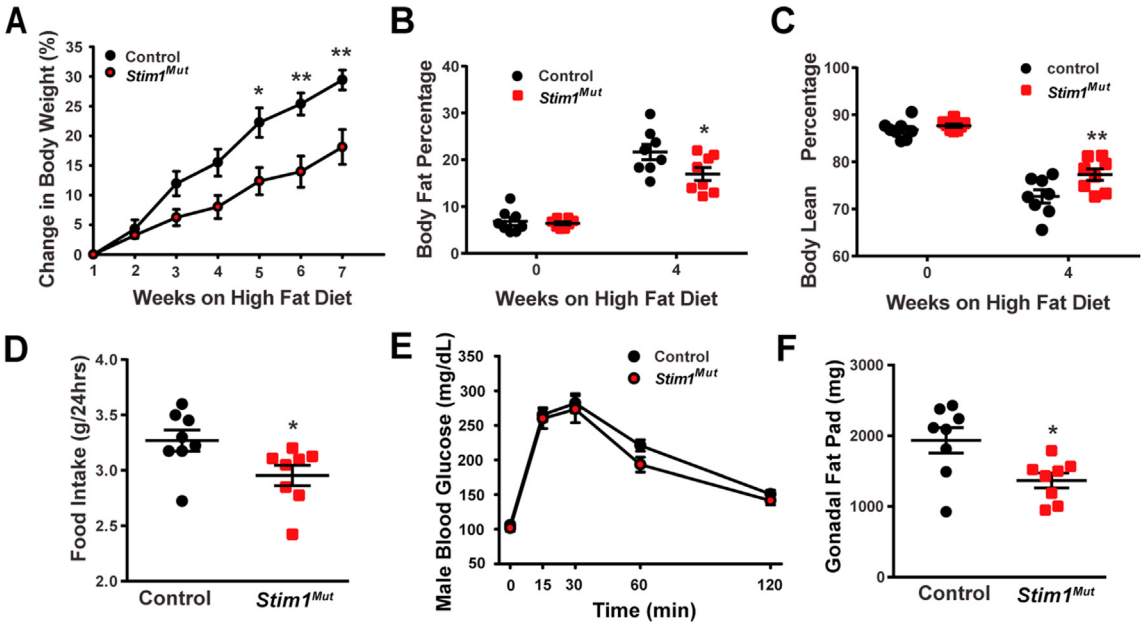


**Figure 5: *Stim1* mutagenesis in POMC neurons attenuates body mass, fat, and food intake in mice on a high fat diet.** Male *Pomc*$^{Cre}$ mice were placed on high fat diet (45%) 10 days after being injected with AAV1- FLEX-SaCas9-U6-sg*Stim1* (n = 8) or AAV1-FLEX-SaCas9-U6-sgControl (n = 8). **A**, percent change in body weight measured once a week for seven weeks. The high fat diet caused significant weight gain in both groups relative to their baseline, with the controls gaining significantly more by 5 weeks (two-way ANOVA: main effect of treatment ($F_{(1, 13)} = 7.076$, $p = 0.0196$), main effect of time ($F_{(7, 91)} = 78.14$, $p < 0.0001$) and interaction ($F_{(7, 91)} = 5.341$, $p < 0.0001$); control, $n = 8$, *Stim1*$^{Mut}$, $n = 8$; *post hoc* Bonferroni test, $^{*}p < 0.05$, $^{**}p < 0.01$). Total body fat (**B**) and Lean mass (**C**) measured by an EchoMRI Whole Body Composition Analyzer (Echo Medical Systems, Houston, TX, USA). Lean mass does not include bone and fluids within organs. The difference in body fat percentage (**B**) and lean mass percentage (**C**) between the groups became significantly different by 4 weeks on high fat diet (two-way ANOVA for B: main effect of treatment ($F_{(1, 14)} = 3.092$, $p = 0.1005$), main effect of time ($F_{(1, 14)} = 260.3$, $p < 0.0001$) and interaction ($F_{(1, 14)} = 7.379$, $p = 0.0167$); control, n = 8, *Stim1*$^{Mut}$, $n = 8$; *post hoc* Bonferroni test, $^{*}p < 0.05$. Two-way ANOVA for C: main effect of treatment $F_{(1, 14)} = 5.801$, $p = 0.0304$, main effect of time $F_{(1,14)} = 205.1$, $p < 0.0001$ and interaction ($F_{(1, 14)} = 4.833$, $p = 0.0452$); control, n = 8, *Stim1*$^{Mut}$, n = 8; *post hoc* Bonferroni test, $^{**}p < 0.01$). **D**, five weeks after viral injection, average 24-hour food intake was measured for four consecutive days (representative data shown). *Stim1*$^{Mut}$ significantly reduced food intake (unpaired two-tailed *t*-test of each animal's average, $t_{(14)} = 2.380$, $^{*}p = 0.0321$). **E**, six weeks after viral injection and 5 weeks on high fat diet, the GTTs showed no significant difference between the two groups (two-way ANOVA: main effect of treatment ($F_{(1, 14)} = 0.9184$, $p = 0.35$), main effect of time ($F_{(4, 56)} = 175.5$, $p < 0.0001$) and interaction ($F_{(4, 56)} = 0.7049$, $p = 0.5919$); control, $n = 8$, *Stim1*$^{Mut}$, $n = 8$; *post hoc* Bonferroni test, $p > 0.05$). **F**, Fat pad of *Stim1*$^{Mut}$ mice on high fat diet for 7–8 weeks were 30% lighter than control DIO mice at the time that they were euthanized for electrophysiology studies (unpaired two-tailed *t*-test, $t_{(14)} = 2.724$, $^{*}p = 0.0165$).

homeostasis. Furthermore, CRISPR technology enabled *Stim1* mutagenesis in an adult animal which not only reduced the chance of developmental compensation, but also avoided apparent embryonic lethality.

Over ten years ago, we discovered that leptin and insulin excite/depolarize POMC neurons through activation of TRPC 5 channels [11,12,44,45]. Leptin binds to its receptor (LRb) to activate Jak2, which phosphorylates insulin receptor substrate (IRS) proteins that activate a PI3 kinase signaling pathway [46]. In POMC neurons the insulin receptor (InsR) couples to PI3K p110β activation [47,48], and the insulin receptor-mediated excitation of POMC neurons is abrogated by inhibition of PI3K activity [11,12,48,49]. Activation of PI3K generates $PIP_3$, which stimulates phospholipase C (PLC) and protein kinase B (Akt) [12,50–52]. Subsequently, PLC hydrolyzes $PIP_2$, which ultimately modulates TRPC 5 channel activity [12,53,54]. In addition, PI3K quickly increases the vesicular trafficking of TRPC 5 channels to the plasma membrane to further boost $Ca^{2+}$ entry into neurons [55]. Therefore, insulin appears to have dual complementary actions to directly activate TRPC 5 channels and to mobilize intracellular vesicular pools of TRPC 5 channels to further augment its activity via PI3K signaling pathways in POMC neurons [12,56].

More recently, we uncovered a critical role of STIM1 in the insulin signaling cascade in POMC neurons [15]. TRPC channels form either receptor-operated cation channels (activated by membrane delimited receptors) or store-operated calcium channels (activated by depletion of calcium stores), which is dependent on their association with STIM1 and plasma membrane calcium channels (*e.g.,* TRPC and Orai channels) [8,13,57]. Upon depletion of intracellular (endoplasmic reticulum) $Ca^{2+}$ stores, STIM1 undergoes a conformational change, oligomerizes and then interacts with plasma membrane Orai and TRPC channels to become plasma membrane calcium release-activated calcium channels [13,14,58]. *Stim1* mRNA is highly expressed in POMC neurons (Figure 1) [15], and estradiol downregulates *Stim1* mRNA expression, which is critical for maintaining insulin excitability in POMC neurons with diet-induced obesity [15]. Indeed, in ovariectomized females that are relatively refractory to insulin excitation, bath perfusion of a SOCE inhibitor (GSK7975A) rapidly increases the insulin-mediated excitation of POMC neurons (*i.e.*, activation of the TRPC 5 mediated inward current), which supports the concept that TRPC 5 channels play a role both in SOCE and receptor operated calcium entry [8,13]. Therefore, selective mutagenesis of *Stim1* in POMC neurons would not only enhance the responses to insulin and leptin by rendering TRPC 5 channels as receptor-operated channels, but also would boost the excitatory responses to glutamate via mGluR1/5 (Figure 6) and serotonin via the $5HT_{2C}$ receptor [59].

Downregulating STIM1 decreases the SERCA (sarco/endoplasmic reticulum $Ca^{2+}$-ATPase) -dependent cytosolic $Ca^{2+}$ clearance and elevates intracellular $Ca^{2+}$ levels [31], which could also contribute to

 

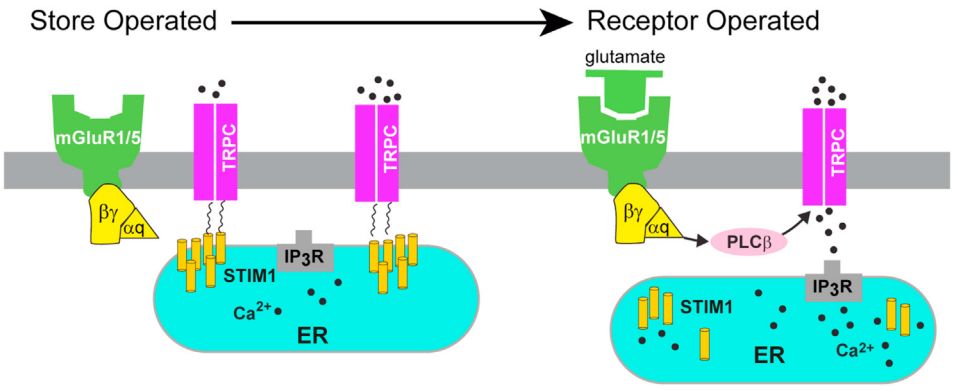


**Figure 6: A cellular model of STIM1 affecting mGluR1/5 activation of TRPC5 channels in POMC neurons.** Store-operated calcium entry (SOCE) is a conserved mechanism by which the depletion of the endoplasmic reticulum (ER) calcium stores is conveyed to calcium-permeable channels at the plasma membrane, triggering calcium influx from the extracellular space and into the cell cytosol. A physiological mechanism responsible for the activation of SOCE results from the stimulation of G protein-coupled receptors associated with the IP3 and phospholipase C cascade, resulting in the release of calcium from ER, via the IP3 receptor (IP3R). **Left panel**, under physiological conditions, STIM1 interacts with TPRC5 channels thereby engaging these $Ca^{2+}$ channels as store-operated channels, which are activated with ER depletion of $Ca^{2+}$. **Right Panel**, however, under certain physiological conditions such as in females where estrogen downregulates the expression of STIM1, TRPC5 channels are converted to receptor-operated channels in POMC neurons. [In this study in males, we used CRISPR/SaCas9 mutagenesis of STIM1 to reduce its expression.] Therefore, glutamate binds to its receptor (mGluR1/5) to activate Gaq—PLCβ signaling cascade to facilitate TPRC5 channel opening, generating a robust inward $Ca^{2+}/Na^{+}$ current to depolarize POMC neurons to increase POMC neuronal excitability.

activation of TRPC 5 channels in POMC neurons [60]. Indeed, we have found that $Ca^{2+}$ significantly potentiates the leptin-induced TRPC 5 current in POMC neurons [11], which has recently been corroborated in primary cultures of POMC neurons [61]. Moreover, similar to cerebellar Purkinje neurons [31], we measured a significant decrease in the input resistance with *Stim1* deletion, which we believe reflects an increase in distribution of TRPC 5 channels across the plasma membrane and coupling to mGluR1/5 [8]. A similar scenario occurs in cortical neurons and in heterologous cells expressing *Cav1.2* (L-type calcium) channels and *Stim1*, where inhibition of STIM1 augments $Ca^{2+}$ influx through L-type calcium channels [62,63]. Furthermore, deletion of *Stim1* in cardiomyocyte-derived (HL-1) cells increases the peak amplitude and current density of T-type calcium channels and shifts the activation curve toward more negative membrane potentials [64]. Biotinylation assays have revealed that deletion of *Stim1* increases T-type calcium channel surface expression, and co-immunoprecipitation assays suggest that STIM1 directly regulates T-type channel activity [64]. Thus, STIM1 appears to dampen the activity of voltage-gated calcium channels. Importantly, estradiol treatment downregulates *Stim1* expression in the ARH of ovariectomized female mice and guinea pigs [15], which is why we focused on males in this study. In contrast, E2 upregulates *Cav3.1* channel expression and whole cell currents in POMC neurons [65]. Calcium influx via Cav3.1 channels may also facilitate TRPC 5 channel opening in POMC neurons, but this remains to be determined.

Besides the peptides kisspeptin, neurokinin B and dynorphin, $Kiss1^{ARH}$ neurons also co-express the vesicular glutamate transporter 2 (vGluT2) [27,66], and we have documented that optogenetic stimulation of $Kiss1^{ARH}$ neurons expressing channelrhodopsin releases glutamate, which is dependent on the estrogenic state of females [7]. Although the mRNA expression of *Kiss1, Tac2 and Pdyn* mRNA in $Kiss1^{ARH}$ neurons are all down-regulated by E2 [67,68], *Vglut2* mRNA expression is upregulated together with increased probability of glutamate release in E2 treated, ovariectomized females [7]. Low frequency (1—2 Hz) optogenetic stimulation of $Kiss1^{ARH}$ neurons evokes fast ionotropic glutamatergic EPSCs in POMC and AgRP neurons, but high frequency (20 Hz) optogenetic stimulation releases enough glutamate to induce a slow excitatory response in POMC neurons but a slow inhibitory response in AgRP neurons [7,27,56]. Indeed, the group I mGluR agonist DHPG depolarizes POMC neurons, while group II/III mGluR agonists hyperpolarize AgRP neurons [7]. As opposed to Group I mGluRs (mGluR1 and mGluR5) coupling to $G\alpha_{q/11,}$ group II/III mGluRs (mGluR2 and mGluR7) are $G\alpha_{i/o}$-coupled [69]. Hence, the output of $Kiss1^{ARH}$ neurons excites the anorexigenic POMC neurons and inhibits the orexigenic AgRP neurons. Therefore, $Kiss1^{ARH}$ neurons appear to be an integral part of an anorexigenic circuit in the hypothalamus [7,70,71] [72], which funnels through TRPC 5 signaling in POMC neurons. Besides the glutamatergic projections from the local ARH (kisspeptin) neurons there are glutamatergic inputs from the ventromedial nucleus that are highly regulated by energy states [73—77] that may also signal via mGluR1/5 and be similarly augmented by STIM1 downregulation.

Presently, we have been able to assess a specific function of *Stim1* in ARH-POMC neurons in the adult male. Our attempts to conditionally knockout Stim1 in POMC cells failed perhaps due to the fact POMC is not only expressed in neurons but pituitary corticotrophs [78]. Therefore, we took advantage of CRISPR technology [17,18] utilizing a sgRNA to selectively mutagenize *Stim1* in adult ARH-POMC neurons in male mice. Importantly, there is not a pharmacological approach to inhibit STIM1 signaling in adult animals (*e.g.*, using the SOCE inhibitor GSK7975A) since Stim1 is ubiquitously expressed both in neurons and non-neuronal cells [13,14]. Reduced *Stim1* mRNA expression in POMC neurons was associated with reduced food intake, attenuated weight gain and reduced body fat and fat pad mass in male mice fed a high fat diet. Although we focused on the glutamatergic signaling via mGluR1/5 at the cellular level, the metabolic phenotype would compel one to investigate the effects of insulin and leptin, both of which signal via TRPC5 channels at the plasma membrane [11,12,59]. Indeed, the neuroprotective effects of *Stim1* mutagenesis could be driven, in part, by enhanced insulin/leptin signaling in POMC neurons, which needs to be addressed in future experiments.

## AUTHOR CONTRIBUTIONS

JQ performed and analyzed the electrophysiology experiments. MAB did the single cell harvesting and quantitative PCR analysis of the

 

harvested cells. TLS did the calcium imaging experiments. LSZ and ACH designed and characterized the sgRNA for *Stim1*. JQ, OKR and MJK designed the experiments, analyzed the data and wrote the manuscript with input from the other authors.

## DECLARATIONS OF INTEREST

None.

## DATA AVAILABILITY

Data will be made available on request.

## ACKNOWLEDGEMENTS

We thank Ashely M. Connors for her excellent technical support. This research was funded by US National Institute of Health (NIH) grants: NS038809 (to MJK), NS043330 (to OKR), DK068098 (to MJK and OKR) and DA044315 (to LSZ). We would also like to acknowledge the University of Washington Molecular Genetics Resource Core (P30DA048736, LSZ).

## CONFLICT OF INTEREST

None declared.

## REFERENCES

[1] Clapham DE. TRP channels as cellular sensors. Nature 2003;426:517–24. https://doi.org/10.1038/nature02196.

[2] Ambudkar IS, Ong HL. Organization and function of TRPC channelsomes. Pflueg Arch Eur J Physiol 2007;455(2):187–200. https://doi.org/10.1007/s00424-007-0252-0.

[3] Tozzi A, Bengtson CP, Longone P, Carignani C, Fusco FR, Bernardi G, et al. Involvement of transient receptor potential-like channels in responses to mGluR-I activation in midbrain dopamine neurons. Eur J Neurosci 2003;18(8):2133–45. https://doi.org/10.1046/j.1460-9568.2003.02936.x.

[4] Bengtson CP, Tozzi A, Bernardi G, Mercuri NB. Transient receptor potential-like channels mediate metabotropic glutamate receptor EPSCs in rat dopamine neurones. J Physiol 2004;555(Pt 2):323–30. https://doi.org/10.1113/jphysiol.2003.060061.

[5] Berg AP, Sen N, Bayliss DA. TrpC3/C7 and Slo2.1 are molecular targets for metabotropic glutamate receptor signaling in rat striatal cholinergic interneurons. J Neurosci 2007;27(33):8845–56. https://doi.org/10.1523/JNEUROSCI.0551-07.2007.

[6] Faber ES, Sedlak P, Vidovic M, Sah P. Synaptic activation of transient receptor potential channels by metabotropic glutamate receptors in the lateral amygdala. Neuroscience 2006;137(3):781–94. https://doi.org/10.1016/j.neuroscience.2005.09.027.

[7] Qiu J, Rivera HM, Bosch MA, Padilla SL, Stincic TL, Palmiter RD, et al. Estrogenic-dependent glutamatergic neurotransmission from kisspeptin neurons governs feeding circuits in females. Elife 2018;7:e35656. https://doi.org/10.7554/eLife.35656.

[8] Birnbaumer L. The TRPC class of ion channels: a critical review of their roles in slow, sustained increases in intracellular $Ca^{2+}$ concentrations. Annu Rev Pharmacol Toxicol 2009;49:395–426. https://doi.org/10.1146/annurev.pharmtox.48.113006.094928.

[9] Venkatachalam K, Montell C. TRP channels. Annu Rev Biochem 2007;76:387–417. https://doi.org/10.1146/annurev.biochem.75.103004.142819.

[10] Clapham DE, Julius D, Montell C, Schultz G. International Union of Pharmacology. XLIX. Nomenclature and structure-function relationships of transient receptor potential channels. Pharmacol Rev 2005;57(4):427–50. https://doi.org/10.1124/pr.57.4.6.

[11] Qiu J, Fang Y, Rønnekleiv OK, Kelly MJ. Leptin excites proopiomelanocortin neurons via activation of TRPC channels. J Neurosci 2010;30(4):1560–5. https://doi.org/10.1523/JNEUROSCI.4816-09.2010.

[12] Qiu J, Zhang C, Borgquist A, Nestor CC, Smith AW, Bosch MA, et al. Insulin excites anorexigenic proopiomelanocortin neurons via activation of canonical transient receptor potential channels. Cell Metabol 2014;19(4):682–93. https://doi.org/10.1016/j.cmet.2014.03.004.

[13] Salido GM, Jardin I, Rosado JA. The TRPC ion channels: association with Orai1 and STIM1 proteins and participation in capacitative and non-capacitative calcium entry. Adv Exp Med Biol 2011;704:413–33. https://doi.org/10.1007/978-94-007-0265-3_23.

[14] Yuan JP, Zeng W, Huang GN, Worley PF, Muallem S. STIM1 heteromultimerizes TRPC channels to determine their function as store-operated channels. Nat Cell Biol 2007;9(6):636–45. https://doi.org/10.1038/ncb1590.

[15] Qiu J, Bosch MA, Meza C, Navarro UV, Nestor CC, Wagner EJ, et al. Estradiol protects proopiomelanocortin neurons against insulin resistance. Endocrinology 2018;159(2):647–64. https://doi.org/10.1210/en.2017-00793.

[16] Qiu J, Stincic TL, Bosch MA, Connors AM, Petrie SK, Rønnekleiv OK, et al. Deletion of Stim1 in hypothalamic arcuate nucleus Kiss1 neurons potentiates synchronous GCaMP activity and protects against diet-induced obesity. J Neurosci 2021;41:9688–701. https://doi.org/10.1523/JNEUROSCI.0622-21.2021.

[17] Hunker AC, Soden ME, Krayushkina D, Heymann G, Awatramani R, Zweifel LS. Conditional single vector CRISPR/SaCas9 viruses for efficient mutagenesis in the adult mouse nervous system. Cell Rep 2020;30(12):4303–16. https://doi.org/10.1016/j.celrep.2020.02.092. e6.

[18] Stincic TL, Bosch MA, Hunker AC, Juarez B, Connors AM, Zweifel LS, et al. CRISPR knockdown of Kcnq3 attenuates the M current and increases excitability of NPY/AgRP neurons to alter energy balance. Mol Metabol 2021;49:101218. https://doi.org/10.1016/j.molmet.2021.101218.

[19] Balthasar N, Coppari R, McMinn J, Liu SM, Lee CE, Tang V, et al. Leptin receptor signaling in POMC neurons is required for normal body weight homeostasis. Neuron 2004;42:983–91.

[20] Cowley MA, Smart JL, Rubinstein M, Cerdán MG, Diano S, Horvath TL, et al. Leptin activates anorexigenic POMC neurons through a neural network in arcuate nucleus. Nature 2001;411(6836):480–4. https://doi.org/10.1038/35078085.

[21] Oh-hora M, Yamashita M, Hogan PG, Sharma S, Lamperti E, Chung W, et al. Dual functions for the endoplasmic reticulum calcium sensors STIM1 and STIM2 in T cell activation and tolerance. Nat Immunol 2008;9(4):432–43. https://doi.org/10.1038/ni1574.

[22] Bäckman CM, Malik N, Zhang Y, Shan L, Grinberg A, Hoffer BJ, et al. Characterization of a mouse strain expressing Cre recombinase from the 3′ untranslated region of the dopamine transporter locus. Genesis 2006;44(8):383–90. https://doi.org/10.1002/dvg.20228.

[23] Parton LE, Ye CP, Coppari R, Enriori PJ, Choi B, Zhang C-Y, et al. Glucose sensing by POMC neurons regulates glucose homeostasis and is impaired in obesity. Nature 2007;449:228–32.

[24] Paeger L, Pippow A, Hess S, Paehler M, Klein AC, Husch A, et al. Energy imbalance alters $Ca^{2+}$ handling and excitability of POMC neurons. Elife 2017;6:1–21. https://doi.org/10.7554/eLife.25641.

[25] Ayala JE, Samuel VT, Morton GJ, Obici S, Croniger CM, Shulman GI, et al. Standard operating procedures for describing and performing metabolic tests of glucose homeostasis in mice. Disease Models & Mechanisms 2010;3(9–10):525–34. https://doi.org/10.1242/dmm.006239.

[26] Bosch MA, Tonsfeldt KJ, Rønnekleiv OK. mRNA expression of ion channels in GnRH neurons: subtype-specific regulation by 17β-Estradiol. Mol Cell Endocrinol 2013;367(1–2):85–97. https://doi.org/10.1016/j.mce.2012.12.021.

  

[27] Nestor CC, Qiu J, Padilla SL, Zhang C, Bosch MA, Fan W, et al. Optogenetic stimulation of arcuate nucleus Kiss1 neurons reveals a steroid-dependent glutamatergic input to POMC and AgRP neurons in male mice. Mol Endocrinol 2016;30(6):630—44. https://doi.org/10.1210/me.2016-1026.

[28] Livak KJ, Schmittgen TD. Analysis of relative gene expression data using real-time quantitative PCR and the $2^{-\Delta\Delta CT}$ method. Methods 2001;25(4):402—8. https://doi.org/10.1006/meth.2001.1262.

[29] Pfaffl MW. A new mathematical model for relative quantification in real-time RT-PCR. Nucleic Acids Res 2001;29(9):e45. https://doi.org/10.1093/nar/29.9.e45.

[30] Hartmann J, Karl RM, Alexander RP, Adelsberger H, Brill MS, Rühlmann C, et al. STIM1 controls neuronal $Ca^{2+}$ signaling, mGluR1-dependent synaptic transmission, and cerebellar motor behavior. Neuron 2014;82(3):635—44. https://doi.org/10.1016/j.neuron.2014.03.027.

[31] Ryu C, Jang DC, Jung D, Kim YG, Shim HG, Ryu H-H, et al. STIM1 regulates somatic $Ca^{2+}$ signals and intrinsic firing properties of cerebellar Purkinje neurons. J Neurosci 2017;37(37):8876. https://doi.org/10.1523/JNEUROSCI.3973-16.2017.

[32] Sun Y, Zhang H, Selvaraj S, Sukumaran P, Lei S, Birnbaumer L, et al. Inhibition of L-Type $Ca^{2+}$ channels by TRPC1-STIM1 complex is essential for the protection of dopaminergic neurons. J Neurosci 2017;37(12):3364—77. https://doi.org/10.1523/JNEUROSCI.3010-16.2017.

[33] Deltcheva E, Chylinski K, Sharma CM, Gonzales K, Chao Y, Pirzada ZA, et al. CRISPR RNA maturation by trans-encoded small RNA and host factor RNase III. Nature 2011;471(7340):602—7. https://doi.org/10.1038/nature09886.

[34] Jinek M, Chylinski K, Fonfara I, Hauer M, Doudna JA, Charpentier E. A programmable dual-RNA-guided DNA endonuclease in adaptive bacterial immunity. Science (New York, N.Y.) 2012;337(6096):816—21. https://doi.org/10.1126/science.1225829.

[35] Cong L, Ran FA, Cox D, Lin S, Barretto R, Habib N, et al. Multiplex genome engineering using CRISPR/Cas systems. Science (New York, N.Y.) 2013;339(6121):819—23. https://doi.org/10.1126/science.1231143.

[36] Iyer V, Boroviak K, Thomas M, Doe B, Riva L, Ryder E, et al. No unexpected CRISPR-Cas9 off-target activity revealed by trio sequencing of gene-edited mice. PLoS Genet 2018;14(7):e1007503. https://doi.org/10.1371/journal.pgen.1007503.

[37] Luo X, He Y, Zhang C, He X, Yan L, Li M, et al. Trio deep-sequencing does not reveal unexpected off-target and on-target mutations in Cas9-edited rhesus monkeys. Nat Commun 2019;10(1):5525. https://doi.org/10.1038/s41467-019-13481-y.

[38] Fellinger L, Jo YS, Hunker AC, Soden ME, Elum J, Juarez B, et al. A midbrain dynorphin circuit promotes threat generalization. Curr Biol 2021;31(19):4388—96. https://doi.org/10.1016/j.cub.2021.07.047. e5.

[39] Stincic TL, Grachev P, Bosch MA, Rønnekleiv OK, Kelly MJ. 2018. Estradiol drives the anorexigenic activity of proopiomelanocortin neurons in female mice. eNeuro 2018;5(4):e0103—18. https://doi.org/10.1523/eneuro.0103-18.2018.

[40] Berna-Erro A, Braun A, Kraft R, Kleinschnitz C, Schuhmann MK, Stegner D, et al. STIM2 regulates capacitive $Ca^{2+}$ entry in neurons and plays a key role in hypoxic neuronal cell death. Sci Signal 2009;2(93):ra67. https://doi.org/10.1126/scisignal.2000522. ra67.

[41] Gruszczynska-Biegala J, Pomorski P, Wisniewska MB, Kuznicki J. Differential roles for STIM1 and STIM2 in store-operated calcium entry in rat neurons. PLoS One 2011;6(4):e19285. https://doi.org/10.1371/journal.pone.0019285.

[42] Brini M, Calì T, Ottolini D, Carafoli E. Neuronal calcium signaling: function and dysfunction. Cell Mol Life Sci 2014;71(15):2787—814. https://doi.org/10.1007/s00018-013-1550-7.

[43] Just S, Chenard BL, Ceci A, Strassmaier T, Chong JA, Blair NT, et al. Treatment with HC-070, a potent inhibitor of TRPC4 and TRPC5, leads to anxiolytic and antidepressant effects in mice. PLoS One 2018;13(1):e0191225. https://doi.org/10.1371/journal.pone.0191225.

[44] Qiu J, Fang Y, Bosch MA, Rønnekleiv OK, Kelly MJ. Guinea pig kisspeptin neurons are depolarized by leptin via activation of TRPC channels. Endocrinology 2011;152(4):1503—14. https://doi.org/10.1210/en.2010-1285.

[45] Kelly MJ, Qiu J, Rønnekleiv OK. TRPCing around the hypothalamus. Front Neuroendocrinol 2018;51:116—24. https://doi.org/10.1016/j.yfrne.2018.05.004.

[46] Morton GJ, Gelling RW, Niswender KD, Morrison CD, Rhodes CJ, Schwartz MW. Leptin regulates insulin sensitivity via phosphatidylinositol-3-OH kinase signaling in mediobasal hypothalamic neurons. Cell Metabol 2005;2(6):411—20. https://doi.org/10.1016/j.cmet.2005.10.009.

[47] Xu AW, Kaelin CB, Takeda K, Akira S, Schwartz MW, Barsh GS. PI3K integrates the action of insulin and leptin on hypothalamic neurons. J Clin Invest 2005;115(4):951—8. https://doi.org/10.1172/JCI24301.

[48] Al-Qassab H, Smith MA, Irvine EE, Guillermet-Guibert J, Claret M, Choudhury AI, et al. Dominant role of the p110β isoform of PI3K over p110α in energy homeostasis regulation by POMC and AgRP neurons. Cell Metabol 2009;10(5):343—54. https://doi.org/10.1016/j.cmet.2009.09.008.

[49] Hill JW, Williams KW, Ye C, Luo J, Balthasar N, Coppari R, et al. Acute effects of leptin require PI3K signalng in hypothalamic proopiomelanocortin neurons in mice. J Clin Invest 2008;118(5):1796—805. https://doi.org/10.1172/JCI32964.

[50] Rameh LE, Rhee SG, Spokes K, Kazlauskas A, Cantley LC, Cantley LG. Phosphoinositide 3-kinase regulates phospholipase Cγ-mediated calcium signaling. J Biol Chem 1998;273(37):23750—7. https://doi.org/10.1074/jbc.273.37.23750.

[51] Falasca M, Logan SK, Lehto VP, Baccante G, Lemmon MA, Schlessinger J. Activation of phospholipase Cγ by PI 3-kinase-induced PH domain-mediated membrane targeting. EMBO J 1998;17(2):414—22. https://doi.org/10.1093/emboj/17.2.414.

[52] Bae YS, Cantley LG, Chen C-S, Kim S-R, Kwon K-S, Rhee SG. Activation of phospholipase C-γ by phosphatidylinositol 3,4,5-trisphosphate. J Biol Chem 1998;273(8):4465—9. https://doi.org/10.1074/jbc.273.8.4465.

[53] Rodríguez-Menchaca AA, Adney SK, Zhou L, Logothetis DE. Dual regulation of voltage-sensitive ion channels by $PIP_2$. Front Pharmacol 2012;3:170. https://doi.org/10.3389/fphar.2012.00170. 170.

[54] Zhang C, Bosch MA, Rønnekleiv OK, Kelly MJ. Kisspeptin activation of TRPC4 channels in female GnRH neurons requires $PIP_2$ depletion and cSrc kinase activation. Endocrinology 2013;154(8):2772—83. https://doi.org/10.1210/en.2013-1180.

[55] Bezzerides VJ, Ramsey IS, Kotecha S, Greka A, Clapham DE. Rapid vesicular translocation and insertion of TRP channels. Nat Cell Biol 2004;6(8):709—20. https://doi.org/10.1038/ncb1150.

[56] Qiu J, Nestor CC, Zhang C, Padilla SL, Palmiter RD, Kelly MJ, et al. High-frequency stimulation-induced peptide release synchronizes arcuate kisspeptin neurons and excited GnRH neurons. Elife 2016;5:e16246. https://doi.org/10.7554/eLife.16246.

[57] Wang H, Cheng X, Tian J, Xiao Y, Tian T, Xu F, et al. TRPC channels: structure, function, regulation and recent advances in small molecular probes. Pharmacol Ther 2020;209:107497. https://doi.org/10.1016/j.pharmthera.2020.107497.

[58] Huang GN, Zeng W, Kim JY, Yuan JP, Han L, Muallem S, et al. STIM1 carboxyl-terminus activates native SOC, $I_{crac}$ and TRPC1 channels. Nat Cell Biol 2006;8(9):1003—10. https://doi.org/10.1038/ncb1454.

[59] Gao Y, Yao T, Deng Z, Sohn J-W, Sun J, Huang Y, et al. TrpC5 mediates acute leptin and serotonin effects via *Pomc* neurons. Cell Rep 2017;18(3):583—92. https://doi.org/10.1016/j.celrep.2016.12.072.

[60] Blair NT, Kaczmarek JS, Clapham DE. Intracellular calcium strongly potentiates agonist-activated TRPC5 channels. J Gen Physiol 2009;133(5):525—46. https://doi.org/10.1085/jgp.200810153.

[61] Perissinotti PP, Martínez-Hernández E, Piedras-Rentería ES. TRPC1/5-Cav3 complex mediates leptin-induced excitability in hypothalamic neurons. Front Neurosci 2021;15:1—13. https://doi.org/10.3389/fnins.2021.679078.


 

[62] Park CY, Shcheglovitov A, Dolmetsch R. The CRAC channel activator STIM1 binds and inhibits L-type voltage-gated calcium channels. Science 2010;330(6000):101—5. https://doi.org/10.1126/science.1191027.

[63] Wang Y, Deng X, Mancarella S, Hendron E, Eguchi S, Soboloff J, et al. The calcium store sensor, STIM1, reciprocally controls Orai and CaV1.2 channels. Science 2010;330(6000):105—9. https://doi.org/10.1126/science.1191086.

[64] Nguyen N, Biet M, Simard É, Bèliveau É, Francoeur N, Guillemette G, et al. STIM1 participates in the contractile rhythmicity of HL-1 cells by moderating T-type $Ca^{2+}$ channel activity. Biochim Biophys Acta 2013;1833(6):1294—303. https://doi.org/10.1016/j.bbamcr.2013.02.027.

[65] Qiu J, Bosch MA, Jamali K, Xue C, Kelly MJ, Rønnekleiv OK. Estrogen upregulates T-type calcium channels in the hypothalamus and pituitary. J Neurosci 2006;26(43):11072—82. https://doi.org/10.1523/JNEUROSCI.3229-06.2006.

[66] Cravo RM, Margatho LO, Osborne-Lawrence S, Donato JJ, Atkin S, Bookout AL, et al. Characterization of *Kiss1* neurons using transgenic mouse models. Neuroscience 2011;173:37—56. https://doi.org/10.1016/j.neuroscience.2010.11.022.

[67] Navarro VM, Gottsch ML, Chavkin C, Okamura H, Clifton DK, Steiner RA. Regulation of gonadotropin-releasing hormone secretion by kisspeptin/dynorphin/neurokinin B neurons in the arcuate nucleus of the mouse. J Neurosci 2009;29(38):11859—66. https://doi.org/10.1523/JNEUROSCI.1569-09.2009.

[68] Lehman MN, Coolen LM, Goodman RL. Minireview: kisspeptin/neurokinin B/dynorphin (KNDy) cells of the arcuate nucleus: a central node in the control of gonadotropin-releasing hormone secretion. Endocrinology 2010;151(8):3479—89. https://doi.org/10.1210/en.2010-0022.

[69] Niswender CM, Conn PJ. Metabotropic glutamate receptors: physiology, pharmacology, and disease. Annu Rev Pharmacol Toxicol 2010;50:295—322. https://doi.org/10.1146/annurev.pharmtox.011008.145533.

[70] Rønnekleiv OK, Qiu J, Kelly MJ. Arcuate kisspeptin neurons coordinate reproductive activities with metabolism. Semin Reprod Med 2019;37(3):131—40. https://doi.org/10.1055/s-0039-3400251.

[71] Navarro VM. Metabolic regulation of kisspeptin — the link between energy balance and reproduction. Nat Rev Endocrinol 2020;16:407—20. https://doi.org/10.1038/s41574-020-0363-7.

[72] Stincic TL, Kelly MJ. Estrogenic regulation of reproduction and energy homeostasis by a triumvirate of hypothalamic arcuate neurons. J Neuroendocrinol 2022:e13145. https://doi.org/10.1111/jne.13145.

[73] Pinto S, Roseberry AG, Liu H, Diano S, Shanabrough M, Cai X, et al. Rapid rewiring of arcuate nucleus feeding circuits by leptin. Science 2004;304(5667):110—5. https://doi.org/10.1126/science.1089459.

[74] Sternson SM, Shepherd GMG, Friedman JM. Topographic mapping of VMH-› arcuate nucleus microcircuits and their reorganization by fasting. Nat Neurosci 2005;8:1356—63.

[75] Horvath TL. Synaptic plasticity in energy balance regulation. Obesity 2006;14(Suppl 5):228S—33S. https://doi.org/10.1038/oby.2006.314.

[76] Conde K, Fabelo C, Krause WC, Propst R, Goethel J, Fischer D, et al. Testosterone rapidly augments retrograde endocannabinoid signaling in proopiomelanocortin neurons to suppress glutamatergic input from steroidogenic factor 1 neurons via upregulation of diacylglycerol lipase-α. Neuroendocrinology 2017;105(4):341—56. https://doi.org/10.1159/000453370.

[77] Rau AR, Hentges ST. Energy state alters regulation of proopiomelanocortin neurons by glutamatergic ventromedial hypothalamus neurons: pre- and postsynaptic mechanisms. J Neurophysiol 2021;125(3):720—30. https://doi.org/10.1152/jn.00359.2020.

[78] Gee CE, Chen CL, Roberts JL, Thompson R, Watson SJ. Identification of proopiomelanocortin neurones in rat hypothalamus by *in situ* cDNA-mRNA hybridization. Nature 1983;306(5941):374—6.

 